PUBLISHED VERSION

Aoki, Yasumichi; Blum, Tom; Lin, Huey-Wen; Ohta, Shigemi; Sasaki, Shoichi; Tweedie, Robert; Zanotti, James Michael; Yamazaki, Takeshi; RBC Collaboration; UKQCD Collaboration
Nucleon isovector structure functions in (2+1)-flavor QCD with domain wall fermions
Physical Review. D. Particles, Fields, Gravitation and Cosmology, 2010; 82(1):014501:1-014501:14

© 2010 The American Physical Society

http://prd.aps.org/abstract/PRD/v82/i1/e014501

PERMISSIONS

http://publish.aps.org/authors/transfer-of-copyright-agreement

"The author(s), and in the case of a Work Made For Hire, as defined in the U.S. Copyright Act, 17 U.S.C.

§101, the employer named [below], shall have the following rights (the "Author Rights"):

[...]

3. The right to use all or part of the Article, including the APS-prepared version without revision or modification, on the author(s)' web home page or employer's website and to make copies of all or part of the Article, including the APS-prepared version without revision or modification, for the author(s)' and/or the employer's use for educational or research purposes."

26th April 2013

http://hdl.handle.net/2440/76503

Nucleon isovector structure functions in (2 + 1)-flavor QCD with domain wall fermions

Yasumichi Aoki (青木保道),[1] Tom Blum,[2] Huey-Wen Lin (林慧雯),[3] Shigemi Ohta (太田滋生),[4] Shoichi Sasaki (佐々木勝一),[5] Robert Tweedie,[6] James Zanotti,[6] and Takeshi Yamazaki (山崎剛)[7]

(RBC and UKQCD Collaborations)

[1]*RIKEN-BNL Research Center, Brookhaven National Laboratory, Upton, New York 11973, USA*
[2]*Physics Department, University of Connecticut, Storrs, Connecticut 06269-3046, USA*
[3]*Department of Physics, University of Washington, Seattle, Washington 98195-1560, USA*
[4]*Institute of Particle and Nuclear Studies, KEK, Tsukuba, Ibaraki 305-0801, Japan,*
Department of Particle and Nuclear Physics, Sokendai Graduate University of Advanced Studies, Hayama, Kanagawa 240-0193, Japan,
and RIKEN-BNL Research Center, Brookhaven National Laboratory, Upton, New York 11973, USA
[5]*Department of Physics, University of Tokyo, Hongo 7-3-1, Tokyo 113-0033, Japan*
[6]*School of Physics and Astronomy, The University of Edinburgh, Edinburgh EH9 3JZ, United Kingdom*
[7]*Center for Computational Sciences, University of Tsukuba, Tsukuba, Ibaraki 305-8577, Japan*
(Received 23 March 2010; published 2 July 2010)

We report on numerical lattice QCD calculations of some of the low moments of the nucleon structure functions. The calculations are carried out with gauge configurations generated by the RBC and UKQCD Collaborations with (2 + 1)-flavors of dynamical domain-wall fermions and the Iwasaki gauge action ($\beta = 2.13$). The inverse lattice spacing is $a^{-1} = 1.73$ GeV, and two spatial volumes of $(2.7\ \mathrm{fm})^3$ and $(1.8\ \mathrm{fm})^3$ are used. The up and down quark masses are varied so the pion mass lies between 0.33 and 0.67 GeV, while the strange mass is about 12% heavier than the physical one. The structure function moments we present include the fully nonperturbatively renormalized isovector quark momentum fraction $\langle x\rangle_{u-d}$, the helicity fraction $\langle x\rangle_{\Delta u-\Delta d}$, and transversity $\langle 1\rangle_{\delta u-\delta d}$, as well as an unrenormalized twist-3 coefficient d_1. The ratio of the momentum to helicity fractions, $\langle x\rangle_{u-d}/\langle x\rangle_{\Delta u-\Delta d}$, does not show dependence on the light quark mass and agrees well with the value obtained from experiment. Their respective absolute values, fully renormalized, show interesting trends toward their respective experimental values at the lightest quark mass. A prediction for the transversity, $0.7 < \langle 1\rangle_{\delta u-\delta d} < 1.1$, in the $\overline{\mathrm{MS}}$ scheme at 2 GeV is obtained. The twist-3 coefficient, d_1, though yet to be renormalized, supports the perturbative Wandzura-Wilczek relation.

DOI: 10.1103/PhysRevD.82.014501 PACS numbers: 11.15.Ha

I. INTRODUCTION

We report numerical lattice quantum chromodynamics (QCD) calculations of some low moments of nucleon structure functions using the lattice gauge ensembles [1] jointly generated by the RIKEN-BNL-Columbia (RBC) and UKQCD Collaborations with "2 + 1" flavors of dynamical domain-wall fermions (DWF) [2–4]. Recently, there has been an increased interest in lattice calculations of these moments (see [5–7] for recent reviews).

The structure functions are measured in deep-inelastic scattering of electrons off a nucleon [8–19], the cross section of which is factorized in terms of leptonic and hadronic tensors, $\propto l_{\alpha\beta}W^{\alpha\beta}$. Since the electron leptonic tensor, $l_{\alpha\beta}$, is known, the cross section provides us with structure information about the target nucleon through the hadronic tensor,

$$W^{\alpha\beta} = i\int d^4x e^{iqx}\langle N|T[J^\alpha(x)J^\beta(0)]|N\rangle. \tag{1}$$

Here, q denotes the spacelike four-momentum transferred to the nucleon from the electron through a virtual photon. The hadronic tensor is decomposed into symmetric unpolarized and antisymmetric polarized parts, $W^{\alpha\beta} = W^{\{\alpha\beta\}} + W^{[\alpha\beta]}$:

$$W^{\{\alpha\beta\}}(x, Q^2) = \left(-g^{\alpha\beta} + \frac{q^\alpha q^\beta}{q^2}\right)F_1(x, Q^2) + \left(P^\alpha - \frac{\nu}{q^2}q^\alpha\right)\left(P^\beta - \frac{\nu}{q^2}q^\beta\right)\frac{F_2(x, Q^2)}{\nu}, \tag{2}$$

$$W^{[\alpha\beta]}(x, Q^2) = i\epsilon^{\alpha\beta\gamma\delta}q_\gamma\left\{\frac{S_\delta}{\nu}[g_1(x, Q^2) + g_2(x, Q^2)] - \frac{(q\cdot S)P_\delta}{\nu^2}g_2(x, Q^2)\right\}, \tag{3}$$

with kinematic variables defined as P_α the nucleon momentum, S_α the spin normalized with the nucleon mass M, $S^2 = -M^2$, $\nu = q\cdot P$, $x = Q^2/2\nu$, and $Q^2 = |q^2|$. The

 © 2010 The American Physical Society

unpolarized structure functions are $F_1(x, Q^2)$ and $F_2(x, Q^2)$, and the polarized, $g_1(x, Q^2)$ and $g_2(x, Q^2)$. Their moments are described in terms of Wilson's operator product expansion:

$$2\int_0^1 dx x^n F_1(x, Q^2) = \sum_{q=u,d} c_{1,n}^{(q)}(\mu^2/Q^2, g(\mu))\langle x^n\rangle_q(\mu) + O(1/Q^2), \quad (4)$$

$$\int_0^1 dx x^{n-1} F_2(x, Q^2) = \sum_{f=u,d} c_{2,n}^{(q)}(\mu^2/Q^2, g(\mu))\langle x^n\rangle_q(\mu) + O(1/Q^2), \quad (5)$$

$$2\int_0^1 dx x^n g_1(x, Q^2) = \sum_{q=u,d} e_{1,n}^{(q)}(\mu^2/Q^2, g(\mu))\langle x^n\rangle_{\Delta q}(\mu) + O(1/Q^2), \quad (6)$$

$$2\int_0^1 dx x^n g_2(x, Q^2) = \frac{1}{2}\frac{n}{n+1} \times \sum_{q=u,d} [e_{2,n}^q(\mu^2/Q^2, g(\mu))d_n^q(\mu) - 2e_{1,n}^q\langle x^n\rangle_{\Delta q}(\mu)] + O(1/Q^2), \quad (7)$$

where the Wilson coefficients, c_1, c_2, e_1, and e_2, are perturbatively known. The moments, $\langle x^n\rangle_q(\mu)$, $\langle x^n\rangle_{\Delta q}(\mu)$, and $d_n^q(\mu)$ are calculable on the lattice as forward nucleon matrix elements of certain local and gauge-invariant operators.

In addition, the tensor charge,

$$\langle 1\rangle_{\delta q}(\mu) = \frac{M}{2(S_\alpha P_\beta - S_\beta P_\alpha)}\langle P, S|\bar{q} i\sigma_{\alpha\beta}\gamma_5 q|P, S\rangle, \quad (8)$$

which probes the transverse spin structure of the nucleon, will soon be reported by experiments [20,21]. This quantity is calculated on the lattice in much the same way as the DIS structure function moments are calculated.

In this paper we report our lattice numerical calculations of the following four moments of the structure functions: the quark momentum fraction $\langle x\rangle_q(\mu)$, the helicity fraction $\langle x\rangle_{\Delta q}(\mu)$, the tensor charge $\langle 1\rangle_{\delta q}(\mu)$, and twist-3 coefficient d_1^q of the g_2 polarized structure function. These are the moments that can be calculated without finite momentum transfer. For the former three moments, the momentum and helicity fractions and tensor charge, we restrict ourselves to the isovector flavor combination, $q = u - d$, as this simplifies nonperturbative renormalization. All three are nonperturbatively renormalized and readily comparable with the corresponding experiments.

The numerical calculations of these moments use the lattice gauge ensembles generated by the RBC and UKQCD Collaborations with $2 + 1$ flavors of dynamical domain-wall fermions. The good chiral and flavor symmetries of DWF make our calculations and analyses straightforward: in contrast to more conventional fermion formalisms, such as staggered or Wilson, there is no question in defining nucleon quantum numbers, nor complications arising from explicit breaking of chiral symmetry. This advantage is especially important in nonperturbatively renormalizing the results so they can be compared with experiment and phenomenology. In this paper we report results from the ensembles with lattice cutoff $a^{-1} = 1.73(3)$ GeV [1]. We consider two spatial volumes, with linear size about 2.7 and 1.8 fm each. The strange quark mass is fixed at a value about 12% heavier than its physical value, and the degenerate up and down quark mass is varied for four values from about three quarter to one fifth of the strange quark mass. Since we only vary the light quark mass in our simulation while the strange quark mass is held fixed, in the following we call the light up and down quark mass m_f, in lattice units, unless explicitly stated otherwise.

The rest of this paper is organized as follows: We explain our computational method in Sec. II. In Sec. III, we first summarize the numerical lattice QCD ensembles used for this work. Then, we discuss in detail the known systematic errors in the relevant form factors calculated on these ensembles. The numerical results are presented in Sec. IV. Finally, we give the conclusions in Sec. V.

We note that some preliminary results from this study were presented in Refs. [22–24].

II. FORMULATION

We refer the reader to our recent publications [25–27] and references cited there in for details of our computational method. Here, we give a brief summary for readers' convenience. We use the standard proton operator, $B = \epsilon_{abc}(u_a^T C\gamma_5 d_b)u_c$ to create and annihilate proton states. We Gaussian-smear this operator for better overlap with the ground state with both zero and finite momentum. A Gaussian radius of 7 lattice units was chosen after a series of pilot calculations. Since the up and down quark mass are degenerate in these calculations, isospin symmetry is exact. This is of course a well-known good approximation. We project onto the positive-parity ground state, so our proton two-point correlation function takes the form

$$C_{2\text{pt}}(t) = \sum_{\alpha,\beta}\left(\frac{1+\gamma_t}{2}\right)_{\alpha\beta}\langle B_\beta(t_{\text{sink}})\bar{B}_\alpha(t_{\text{source}})\rangle, \quad (9)$$

with $t = t_{\text{sink}} - t_{\text{source}}$. We insert an appropriate operator $O(\vec{q}, t')$ at time t', $t_{\text{source}} \le t' \le t_{\text{sink}}$, and possibly finite momentum transfer $\vec{q}$, to obtain a form factor or structure function moment three-point correlation function,

$$C_{3\text{pt}}^{\Gamma,O}(t, t', \vec{q}) = \sum_{\alpha,\beta}\Gamma_{\alpha\beta}\langle B_\beta(t_{\text{sink}})O(\vec{q}, t')\bar{B}_\alpha(t_{\text{source}})\rangle, \quad (10)$$

with appropriate projection, $\Gamma = \frac{1+\gamma_t}{2}$, for a spin-

unpolarized, and $\Gamma = \frac{1+\gamma_t}{2} i\gamma_5\gamma_k$, $k \neq 4$, for a polarized nucleon. Ratios of these two- and three-point functions give plateaus for $0 < \tau = t' - t_{\text{source}} < t$ that are fitted to a constant to extract the bare lattice matrix elements of desired observables: e.g. at $q^2 = 0$, we use the ratio

$$\langle O \rangle^{\text{bare}} = \frac{C_{3\text{pt}}^{\Gamma,O}(t,\tau)}{C_{2\text{pt}}(t)}. \tag{11}$$

In this paper we limit ourselves to those low structure function moments that are calculable at $q^2 = 0$, as are listed in Table I.

The structure function moments are renormalized nonperturbatively using the Rome-Southampton regularization independent (RI-MOM) scheme [28,29]. The chiral symmetry of DWF is relied on to suppress mixing with lattice-artifact operators. The specific procedures for the operators studied in this paper have been described in previous RBC publications [25,26]. Here, we summarize them for the readers' convenience. First, we take the Fourier transform of the Green's function for operator O_Γ constructed from a point-source propagator at the origin,

TABLE I. Operators used in the structure function moment calculations, including the notation for the operator, the explicit operator form, the hypercubic group representation, the correlator ratios, and the projection operators used in the nonperturbative renormalization of the operator in Eq. (17).

Quark momentum fraction $\langle x \rangle_q$	
O_Γ	$\mathcal{O}_{44}^q = \bar{q}[\gamma_4 \overleftrightarrow{D}_4 - \frac{1}{3}\sum_k \gamma_k \overleftrightarrow{D}_k]q$
Hypercubic group rep.	$\mathbf{3}_1^+$
Correlator ratio	$R_{\langle x \rangle_q} = \frac{C_{3\text{pt}}^{\Gamma,\mathcal{O}_{44}^q}}{C_{2\text{pt}}} = m_N \langle x \rangle_q$
Nonperturbative renormalization (NPR) projection	$\mathcal{P}_{44}^{q-1} = \gamma_4 p_4 - \frac{1}{3}\sum_{i=1,3} \gamma_i p_i$
Quark helicity fraction $\langle x \rangle_{\Delta q}$	
O_Γ	$\mathcal{O}_{\{34\}}^{5q} = i\bar{q}\gamma_5[\gamma_3 \overleftrightarrow{D}_4 + \gamma_4 \overleftrightarrow{D}_3]q$
Hypercubic group rep.	$\mathbf{6}_3^-$
Correlator ratio	$R_{\langle x \rangle_{\Delta q}} = \frac{C_{3\text{pt}}^{\Gamma,\mathcal{O}_{\{34\}}^{5q}}}{C_{2\text{pt}}} = m_N \langle x \rangle_{\Delta q}$
NPR projection	$\mathcal{P}_{34}^{5q-1} = i\gamma_5(\gamma_3 p_4 + \gamma_4 p_3)$
Transversity $\langle 1 \rangle_{\delta q}$	
O_Γ	$\mathcal{O}_{34}^{\sigma q} = \bar{q}\gamma_5\sigma_{34}q$
Hypercubic group rep.	$\mathbf{6}_1^+$
Correlator ratio	$R_{\langle 1 \rangle_{\delta q}} = \frac{C_{3\text{pt}}^{\Gamma,\mathcal{O}_{\{34\}}^{\sigma q}}}{C_{2\text{pt}}} = \langle 1 \rangle_{\delta q}$
NPR projection	$\mathcal{P}_{34}^{\sigma q-1} = \gamma_5\sigma_{34}$
Twist-3 matrix element d_1	
O_Γ	$\mathcal{O}_{[34]}^{5q} = i\bar{q}\gamma_5[\gamma_3 \overleftrightarrow{D}_4 - \gamma_4 \overleftrightarrow{D}_3]q$
Hypercubic group rep.	$\mathbf{6}_1^+$
Correlator ratio	$R_{d_1} = \frac{C_{3\text{pt}}^{\Gamma,\mathcal{O}_{[34]}^{5q}}}{C_{2\text{pt}}} = d_1$
NPR projection	$\mathcal{P}_{[34]}^{5q-1} = i\gamma_5(\gamma_3 p_4 - \gamma_4 p_3)$

$$G_{O_\Gamma}(p,p';a) = \sum_{x,y} e^{-ip\cdot x + ip'\cdot y} \langle \psi(x) O_\Gamma(0) \bar{\psi}(y) \rangle, \tag{12}$$

$$= \sum_{x,y} e^{-ip\cdot x + ip'\cdot y} \langle S(x,0) \Gamma S(0,y) \rangle, \tag{13}$$

where O_Γ is one of $\mathcal{O}_{44}^q$, $\mathcal{O}_{34}^{\sigma q}$, $\mathcal{O}_{\{34\}}^{5q}$, or $\mathcal{O}_{[34]}^{5q}$. The needed Fourier-transformed point-source and point-split–source propagators are

$$S(p;a) = \sum_x e^{-ip\cdot x} S(x;0), \tag{14}$$

$$D_\mu S(p;a) = \sum_x \frac{1}{2} e^{-ip\cdot x} [S(x;-\hat{\mu}) U_\mu(-\hat{\mu}) - S(x;\hat{\mu}) U_\mu^\dagger(0)]. \tag{15}$$

Next, the Green's function is amputated, and evaluated for the case of exceptional momenta ($p = p'$),

$$\Lambda_{O_\Gamma}(p;a) = \langle S(p;a)^{-1} \rangle G_{O_\Gamma}(p;p;a) \langle S(p;a)^{-1} \rangle. \tag{16}$$

Z^{RI} is obtained by requiring the renormalized Green's function, after some suitable projection, be equal to its tree-level counterpart [28],

$$Z_{O_\Gamma}(\mu;a)^{-1} Z_q(\mu;a) = \frac{1}{12} \text{Tr}(\Lambda_{O_\Gamma}(p;a) P_\Gamma)|_{p^2=\mu^2}. \tag{17}$$

The projectors for each O_Γ are listed in Table I. Since we wish to match these renormalized operators to the perturbative $\overline{\text{MS}}$ scheme, the renormalization scale μ must be large enough for perturbation theory to be valid, but not so large to introduce lattice artifacts. Thus, μ should satisfy $\Lambda_{\text{QCD}} \ll \mu \ll 1/a$. In practice, we have found that the upper bound is not so strict, and can be replaced by the milder condition that $(pa)^2 < 3$.

Finally, the following steps, similar to those from [26] allow us to convert the renormalization constants to the continuum $\overline{\text{MS}}$ scheme at 2 GeV.

(1) Obtain $Z^{\text{RI}}(\mu)$: The ratio of $Z_{O_\Gamma}(\mu;a)/Z_q(\mu;a)$ to $Z_A/Z_q(\mu;a)$ is computed and yields $Z_{O_\Gamma}(\mu;a)/Z_A$. Each of the factors in the ratio is first extrapolated to the chiral limit, $m_f = -m_{\text{res}}$, at fixed momentum. Using $Z_A = 0.7161$ [1], we can determine $Z_{O_\Gamma}(\mu;a)$ in Eq. (17), the renormalization constant in the RI scheme, which we denote as Z^{RI}.

(2) Convert to $\overline{\text{MS}}$ scheme: We are interested in continuum quantities, mostly calculated in the $\overline{\text{MS}}$ scheme. The conversion factors between RI and $\overline{\text{MS}}$ schemes for the operators discussed here have been calculated in Refs. [30,31]. To get $Z^{\overline{\text{MS}}}(\mu)$, we use $\alpha_s^{(3)}(\mu)$ obtained by numerically solving the renormalization group equation with the four-loop anomalous dimension [32] and initial condition

$\alpha_s^{(5)}(m_Z) = 0.1176$ [33], following the method in Appendix A of Ref. [34].

(3) Running to 2 GeV with two-loop anomalous dimensions [31,35]. This will take away the continuum running factor.

(4) Remove $(ap)^2$ lattice artifacts: We fit the remaining momentum dependence, which we will observe to be very small, to the form $f = A(ap)^2 + B$ and finally get $Z^{\overline{\rm MS}}(2\ {\rm GeV})$.

III. ENSEMBLES

We follow the same sampling procedure as in our nucleon form factor calculations reported in Ref. [27].

A. Statistics

The RBC-UKQCD joint (2 + 1)-flavor dynamical DWF ensembles [1] are used for the calculations. These ensembles are generated with Iwasaki gauge action [36] at the coupling $\beta = 2.13$ which corresponds to the lattice cutoff of $a^{-1} = 1.73(3)$ GeV, which is determined from the Ω^- baryon mass [1].

The dynamical up, down, and strange quarks are described by DWF actions with fifth-dimensional extent of $L_s = 16$ and the domain-wall height of $M_5 = 1.8$. The strange quark mass is set at 0.04 in lattice units and turned out to be about 12% heavier than the physical strange quark, after taking into account the additive correction of the residual mass, $m_{\rm res} = 0.00315$. The degenerate light quark masses in lattice units, 0.005, 0.01, 0.02 and 0.03, correspond to pion masses of about 0.33, 0.42, 0.56, and 0.67 GeV and nucleon masses, 1.15, 1.22, 1.38, and 1.55 GeV.

Two lattice sizes are used for our study, $16^3 \times 32$ and $24^3 \times 64$, corresponding to linear spatial extent of approximately 1.8 and 2.7 fm, respectively. The smaller volume ensembles, calculated only with the heavier three light quark masses, are used for a finite-volume study. On the 16^3 ensembles, we use 3500 trajectories separated by 5 trajectories at $m_f = 0.01$ and 0.02, and by 10 at 0.03. The main results are obtained from the larger volume ensembles with the number of the configurations summarized in Table II.

On the larger volume, at the heavier three quark masses we make four measurements on each configuration with the conventional single source method using $t_{\rm src} = 0$, 16, 32, 48, or 8, 19, 40, 51. At the lightest mass the double-source method [27] is used, and two measurements on each configuration are carried out using the source pairs of (0, 32) and (16, 48), or (8, 40) and (19, 51). We made an additional two measurements on roughly half of the configurations with one or the other source pair. This means that we make four, double-source measurements on almost half of the configurations, while two double-source measurements are carried out on the remaining configurations.

TABLE II. $N_{\rm conf}$, $N_{\rm sep}$, and $N_{\rm meas}$ denote number of gauge configurations, trajectory separation between measurements, and the number of measurements on each configuration, respectively, on the 24^3 ensembles. The table also lists the pion and nucleon mass for each ensemble [27].

m_f	$N_{\rm conf}$	$N_{\rm sep}$	$N_{\rm meas}$	m_π [GeV]	M_N [GeV]
0.005	932[a]	10	4[b]	0.3294(13)	1.154(7)
0.01	356	10	4	0.4164(12)	1.216(7)
0.02	98	20	4	0.5550(12)	1.381(12)
0.03	106	20	4	0.6681(15)	1.546(12)

[a]The total number of configurations is actually 646. We carry out extra measurements on a subset of these (286 configurations) to improve the statistics using different source positions.
[b]Two measurements with the double-source method gives effectively four measurements.

On the smaller volume, a single source is used, however the location of this source is shifted for each successive measurement in the order $(x, y, z, t) = (0, 0, 0, 0)$, (4,4,4,8), (8,8,8,16), (12,12,12,24), reducing autocorrelations.

In order to reduce possible autocorrelations among measurements, they are averaged on each configuration and then blocked into bins of 40 trajectories for the 24^3 ensembles, and 20 trajectories for the 16^3 ensembles. The statistical errors are estimated by the jackknife method on the blocked measurements.

Finally, the nonperturbative renormalization constants were computed on the four 24^3 ensembles, on roughly 50 configurations each, separated by 40 trajectories. The maximum momentum value in units of $2\pi/L_i$ in each direction was 6 (spatial) and 17 (temporal), such that $(pa)^2 < 3$.

B. Correlation functions

The quark propagator is calculated with an antiperiodic boundary condition in the temporal direction, and periodic boundary conditions for the spatial directions. We employ gauge-invariant Gaussian smearing [37,38] at the source with smearing parameters $(N, \omega) = (100, 7)$ which were chosen after a series of pilot calculations. For the calculation of the three-point functions, we use a time separation of 12 time slices between the source and sink operators to reduce effects from excited-state contributions as much as possible.

TABLE III. Bare quark momentum and helicity fractions and their naturally renormalized ratio on the $(2.7\ {\rm fm})^3$ ensemble.

m_f	$\langle x \rangle_{u-d}$	$\langle x \rangle_{\Delta u - \Delta d}$	$\langle x \rangle_{u-d}/\langle x \rangle_{\Delta u - \Delta d}$
0.005	0.201(9)	0.240(13)	0.835(46)
0.01	0.219(9)	0.261(14)	0.842(42)
0.02	0.234(8)	0.286(11)	0.821(40)
0.03	0.231(7)	0.285(10)	0.807(32)

C. Systematic errors

There are several important sources of systematic error that need be considered: finite spatial size of the lattice, excited-state contamination, and nonzero lattice spacing. A chiral-perturbation-theory-inspired analysis of the former for meson observables suggests the dimensionless product, $m_\pi L$, of the calculated pion mass m_π and lattice linear spatial extent L, should be set greater than 4 to ensure that the finite-volume correction is negligible (below 1%), and the available lattice calculations seem to support this. While our present parameters satisfy this condition, we discovered that even our larger volume of $(2.7\ \mathrm{fm})^3$ is insufficient for calculating such important nucleon properties as the axial charge [39] and form factors [27]: As we reduce the light quark mass, eventually to $m_\pi = 330$ MeV and $m_\pi L \sim 4$, finite-size effects become severe, exceeding 10%, at least for these quantities that are measured in elastic processes. Similar finite-size effects may influence the moments of structure functions we are discussing in this paper (studies of finite-volume effects in chiral perturbation theory can be found in [40,41]). On the other hand, since these moments are extracted from experimental observables measured in very different inelastic processes, the finite-size effect may enter differently. It is an important goal of this work to investigate such finite-size effects on the moments of structure functions.

In order to reduce contamination from excited states, it is important to adjust the time separation between the nucleon source and sink appropriately so the resultant nucleon observables are free of contamination from excited states. The separation has to be made longer as the quark mass is decreased. In our previous study with two dynamical flavors of DWF quarks [26] with a similar lattice cutoff of about 1.7 GeV, we saw systematic differences between observables calculated with the shorter time separation of 10, or about 1.16 fm, and longer 12, or 1.39 fm: the differences amount to about 20%, or 2 standard deviations (see Fig. 1.) This would suggest that at the shorter time separation of about 1.2 fm, the excited-state contamination has not decayed sufficiently to guarantee correct calculations for the ground-state observables [23]. While it is desirable to use a longer separation, it cannot be made too long in practice without losing control of statistical errors. In Fig. 2, we present the nucleon effective mass at the lightest quark mass, $m_f = 0.005$. The nucleon signal begins to decay at $t = 12$, or about 1.4 fm: this is about longest distance we can choose without losing the signal. As will be shown in detail in this paper, the bare three-point function signals for this source-sink separation of $t = 12$ are acceptable. For all 3-point correlation functions we use a canonical range of time slices from 4 to 8 to obtain average values for matrix elements. We have checked that changing the range to 5–7 makes very little difference, much less than one statistical standard deviation in almost every case, and never more than one. We note that recently the LHP Collaboration has also looked at this issue in some detail [42] and ends up using a shorter separation of about 1.2 fm.

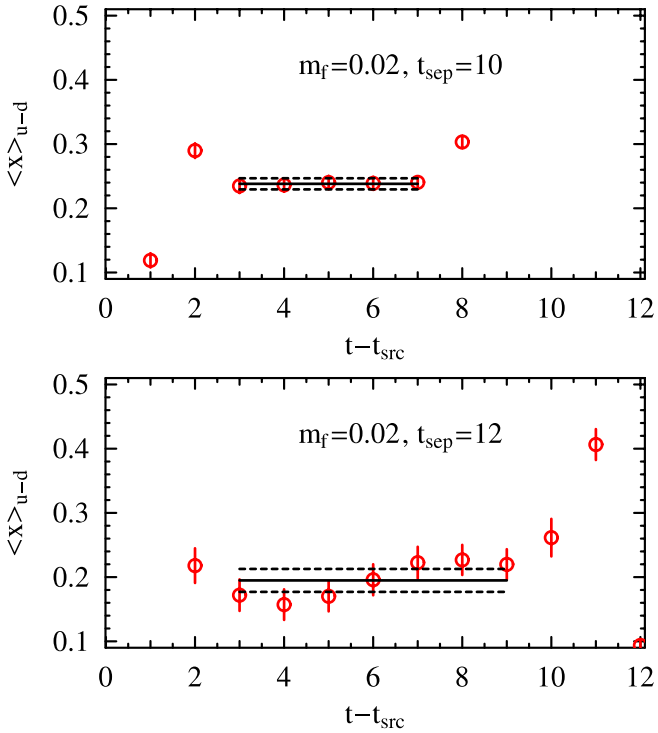

FIG. 1 (color online). A nucleon observable, isovector quark momentum fraction, $\langle x \rangle_{u-d}$, from RBC 2-flavor dynamical DWF ensemble with $m_{ud} = 0.02$ [26], with source-sink separation of 10 and 12: a clear systematic difference is seen. The shorter source-sink separation is not manifestly free of excited-state contamination.

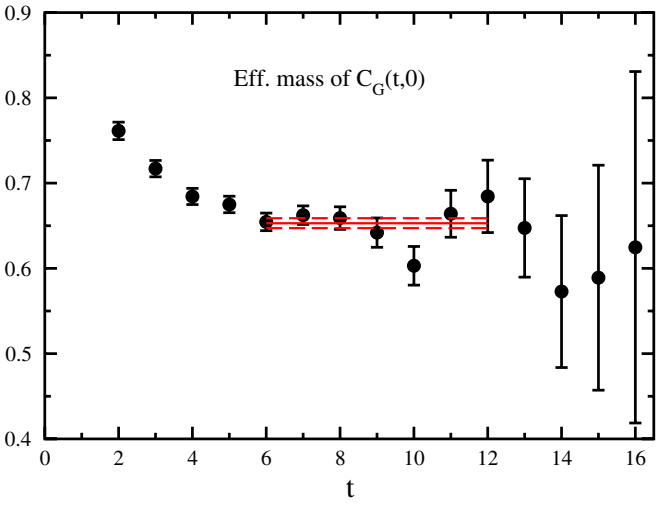

FIG. 2 (color online). Effective mass of the nucleon correlation function with Gaussian smearing applied at both source and sink, for quark mass $m_f = 0.005$.

For low energy quantities like the pseudoscalar decay constants, the kaon B parameter, and the Ω baryon mass, the effect of nonzero lattice spacing was estimated to be less than 4% for the configuration ensemble used in this work [1], and subsequently confirmed on a later ensemble with smaller lattice spacing [43,44]. We expect that similar errors hold for the quantities discussed in this paper. Eventually, a well controlled extrapolation to the continuum limit $a = 0$ will be required. Before doing such an extrapolation, our primary goal is to understand the chiral limit behavior of these matrix elements, which can be done reliably with DWF at nonzero a.

IV. NUMERICAL RESULTS

A. Quark momentum and helicity fractions

Let us first discuss the ratio, $\langle x \rangle_{u-d}/\langle x \rangle_{\Delta u-\Delta d}$, of the isovector quark momentum fraction to the helicity fraction. The momentum fraction, $\langle x \rangle_{u-d}$, which is the first moment of the $F_{1,2}$ unpolarized structure functions, and the helicity fraction, $\langle x \rangle_{\Delta u-\Delta d}$, which is the first moment of the g_1 polarized structure function, share a common renormalization because they are related by a chiral rotation and the DWF action preserves chiral symmetry to a high degree. Thus, this ratio calculated on the lattice is naturally renormalized, much like the form factor ratio [27], g_A/g_V, and is directly comparable with the value obtained from experiment.

The results of our calculation are shown in Fig. 3. They do not show any discernible dependence on the up/down quark mass, outside of the statistical error bars, and are in good agreement with experiment. This is in contrast to the renormalized ratio of g_A/g_V of elastic form factors which at the lightest point deviates significantly from heavier mass results and the experiment as a result of a large finite-size effect [27]. This suggests the moments of inelastic structure functions such as the momentum fraction, $\langle x \rangle_{u-d}$, and helicity fraction, $\langle x \rangle_{\Delta u-\Delta d}$, may not suffer so severely from the finite-size effect that plagues elastic form factor calculations. Indeed the results obtained from the smaller $(1.8\ \mathrm{fm})^3$ volume, also shown in Fig. 3, do not deviate significantly from the constant behavior of the larger volume results, albeit with larger statistical errors.

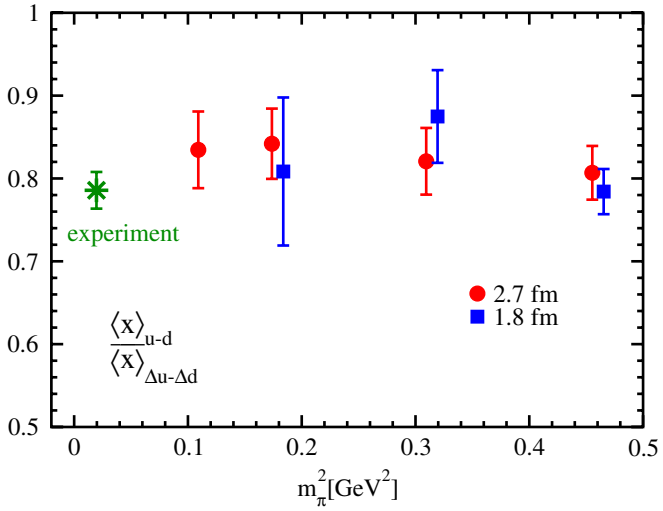

FIG. 3 (color online). Ratio of the bare, isovector, momentum, and helicity fractions, $\langle x \rangle_{u-d}/\langle x \rangle_{\Delta u-\Delta d}$, which is naturally renormalized for DWF. Both volumes are shown, $(2.7\ \mathrm{fm})^3$ (circles) and $(1.8\ \mathrm{fm})^3$ (squares). The square symbols have been moved slightly in the plus x direction. They are in good agreement with experiment which is denoted by the star. No discernible dependence on volume nor pion mass can be detected.

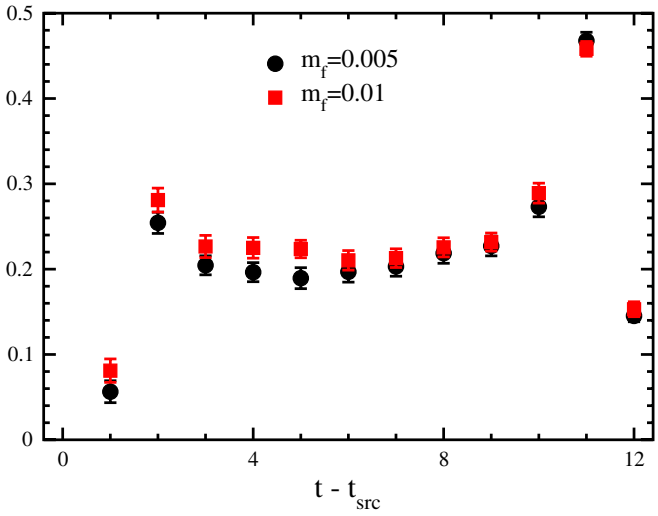

FIG. 4 (color online). Signals for the ratio of three- and two-point functions for the bare quark momentum fraction, $\langle x \rangle_{u-d}$. Quark mass 0.005 (circles) and 0.01 (squares).

Next, we discuss the absolute values of the isovector quark momentum fraction, $\langle x \rangle_{u-d}$. This is the first moment of the unpolarized structure functions, F_1 and F_2. In Fig. 4, we show the bare lattice matrix elements as ratios of three- and two-point functions for the two lightest quark mass values of $m_f = 0.005$ (circles) and 0.01 (squares). We extract bare values of the desired matrix element by averaging over time slices 4 to 8 (values are summarized in Tables III and IV).

These bare values need be renormalized in order to be compared with experiment. In Fig. 5 we present the nonperturbatively determined renormalization for the operator $\mathcal{O}^q_{44}$. The filled circles represent the scale-dependent renor-

TABLE IV. Bare quark momentum and helicity fractions and their naturally renormalized ratio on the $(1.8\ \mathrm{fm})^3$ ensemble.

m_f	$\langle x \rangle_{u-d}$	$\langle x \rangle_{\Delta u-\Delta d}$	$\langle x \rangle_{u-d}/\langle x \rangle_{\Delta u-\Delta d}$
0.01	0.221(18)	0.263(29)	0.808(89)
0.02	0.256(14)	0.291(22)	0.875(56)
0.03	0.236(7)	0.300(11)	0.784(27)

malization constant in the RI-MOM scheme at scale $\mu^2 = p^2$. The filled squares correspond to the renormalization constant given in the $\overline{\text{MS}}$ scheme at $\mu = 2$ GeV, where there remains only residual scale dependence proportional to $(ap)^2$ and $a^2\sum_\mu p_\mu^4/p^2$ lattice artifacts.

Since the RI scheme Z factor for the derivative operator depends not only on p^2, but also on p_ν with ν being the direction of the derivative entering the operator, it has a multiplicity even in the continuum at fixed p^2. When converting Z to the $\overline{\text{MS}}$ scheme, which depends only on $\mu^2 = p^2$, these multiple values at each p^2 are linearly combined with the appropriate matching factors to produce a single value. Because of this averaging, the statistical fluctuations as well as the scatter induced by the $O(4)$ noninvariant artifacts in the $\overline{\text{MS}}$ data are expected to be smaller than that for RI-MOM. This expectation is born out in Fig. 5. In addition, rotational symmetry breaking from nonzero a leads to $O(4)$ noninvariant lattice artifacts proportional to $a^2\sum_\mu p_\mu^4/p^2$ [45–48]. This effect is averaged over though the linear fit used to remove the residual $O((ap)^2)$ artifact, as described in Sec. II. After removing the residual $(ap)^2$ dependence, which is quite small, we obtain a renormalization factor of $Z^{\overline{\text{MS}}}_{\langle x\rangle_q}(2\text{ GeV}) = 1.15(4)$.

To estimate the systematic error on the Z factor stemming from lattice-artifact $O(4)$ symmetry breaking, we repeat the above procedure, but use a restricted range of smaller momenta, which are less susceptible to rotational symmetry breaking. Using the difference in central values from the two fits, $Z^{\overline{\text{MS}}}_{\langle x\rangle_q}(2\text{ GeV})$ increases by about 2%. Adding this error in quadrature to the statistical one, we obtain the final value, $Z^{\overline{\text{MS}}}_{\langle x\rangle_q}(2\text{ GeV}) = 1.15(5)$.

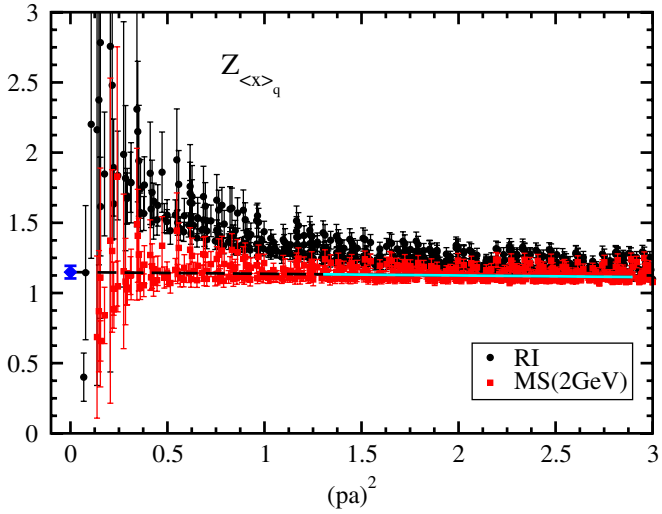

FIG. 5 (color online). Nonperturbative renormalization factor for the quark momentum fraction, $\langle x\rangle_{u-d}$. Circles denote the RI-MOM values, and squares denote the $\overline{\text{MS}}$ ones. The line denotes a linear fit used to remove the leading $O((ap)^2)$ lattice artifacts.

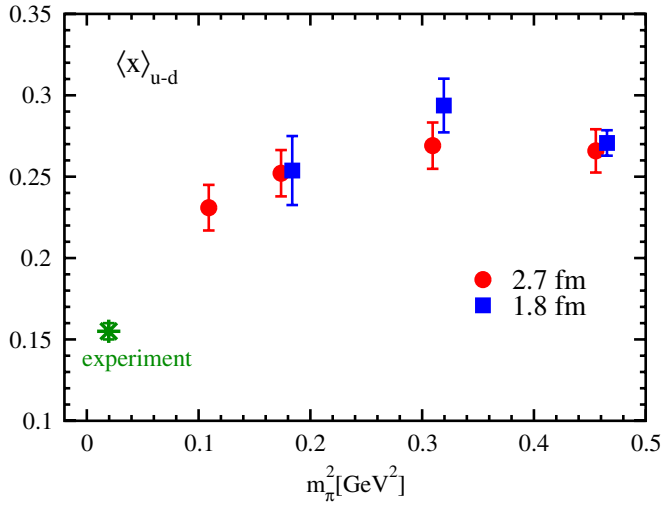

FIG. 6 (color online). Renormalized quark momentum fraction, $\langle x\rangle_{u-d}$. Both volumes are shown, $(2.7\text{ fm})^3$ (circles) and $(1.8\text{ fm})^3$ (squares). The square symbols have been moved slightly in the plus x direction for clarity.

Using this renormalization constant, the quark-mass dependence of the momentum fraction is shown in Fig. 6 and given in Table V. The results from the smaller $(1.8\text{ fm})^3$ volume for the heavier three quark mass values are in agreement with respective mass-value results from the larger volume. These heavier points stay roughly the constant which is about 70% higher at ~0.26 than the experiment, about 0.15. This behavior is not so different from old RBC quenched results [25] and other recent ones [7] with similar up/down quark mass.

On the other hand, the lightest point on the larger $(2.7\text{ fm})^3$ volume, shows a sign of deviation away from this constant behavior. In contrast to the form factor deviations that move away from the experiment in Ref. [27], this one trends toward the experimental value. Since a lighter quark can more easily share its momentum with other degrees of freedom, this trending toward the experiment may well be a real physical effect: It is not necessarily a result of the finite spatial size of the lattice.

Indeed, it is noteworthy that the $m_\pi L$ value of 3.8 for $m_f = 0.01$ at $L = 1.8$ fm is smaller than that of 4.5 for $m_f = 0.005$ at $L = 2.7$ fm. In other words, if there would be such a finite-size effect for this quark momentum fraction that scales with $m_\pi L$ as seen in the form factors, the result from $m_f = 0.01$ at $L = 1.8$ fm should move away from that of $m_f = 0.005$ at $L = 2.7$ fm. We note that in [40] it was predicted that finite-volume effects in $\langle x\rangle_{u-d}$ would only become noticeable for very light quark masses.

The isovector quark helicity fraction, $\langle x\rangle_{\Delta u-\Delta d}$, appears as a leading twist moment of the polarized structure functions g_1 and g_2. Figure 7 presents typical bare signals of this quantity on the larger $(2.7\text{ fm})^3$ volume, for the light-quark mass points $m_f = 0.005$ and 0.01. Average values

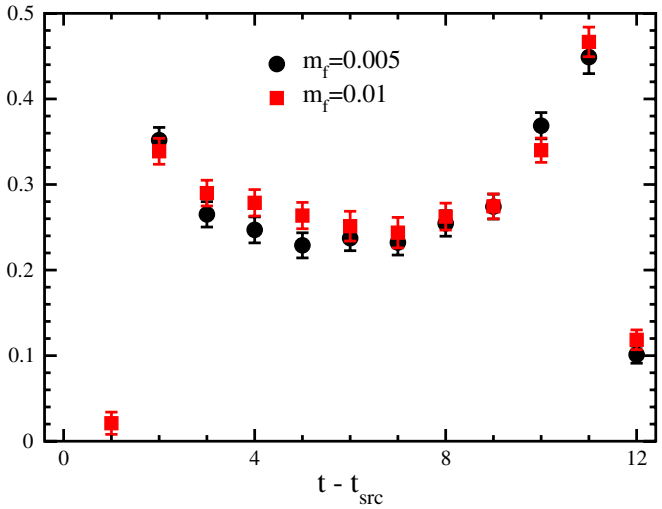

FIG. 7 (color online). Signals for the ratio of three- and two-point functions for the bare quark helicity fraction, $\langle x \rangle_{\Delta u - \Delta d}$. Quark mass 0.005 (circles) and 0.01 (squares).

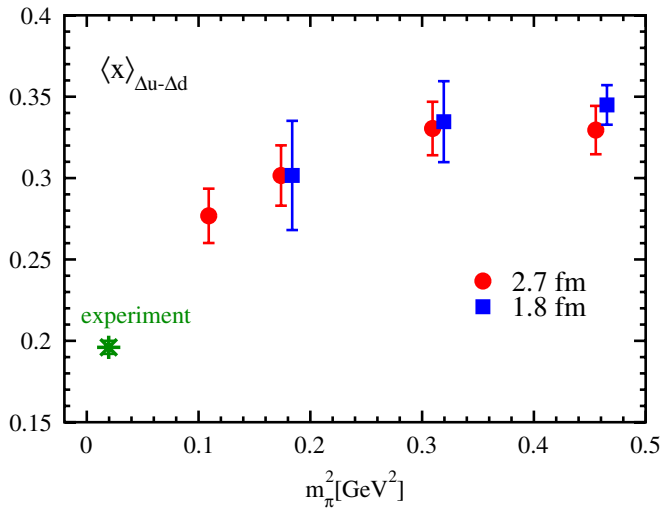

FIG. 9 (color online). The renormalized quark helicity fraction, $\langle x \rangle_{\Delta u - \Delta d}$. Both volumes are shown, $(2.7\ \mathrm{fm})^3$ (circles) and $(1.8\ \mathrm{fm})^3$ (squares). The square symbols have been moved slightly in the plus x direction for clarity.

are extracted as for the momentum fraction, described above. Results are summarized in Table III for the larger volume and Table IV for the smaller volume.

The nonperturbative renormalization of $\langle x \rangle_{\Delta u - \Delta d}$ (for the operator $\mathcal{O}^{5q}_{\{34\}}$), is presented in Fig. 8. We obtain a renormalization factor of $Z^{\overline{\mathrm{MS}}}_{\langle x \rangle_{\Delta q}}(2\ \mathrm{GeV}) = 1.15(3)$ through the same procedure described previously for the momentum fraction. This value agrees very well with the corresponding value for the momentum fraction, as guaranteed by the chiral symmetry of DWF, justifying our use of bare quantities in the ratio, $\langle x \rangle_{u-d}/\langle x \rangle_{\Delta u - \Delta d}$, earlier in this section. Notice the much less pronounced scatter from $O(4)$ noninvariant lattice artifacts in this case, and again, the remarkable flatness of the $\overline{\mathrm{MS}}$ results. The systematic error from $O(4)$ symmetry breaking is negligible compared to the statistical error in this case.

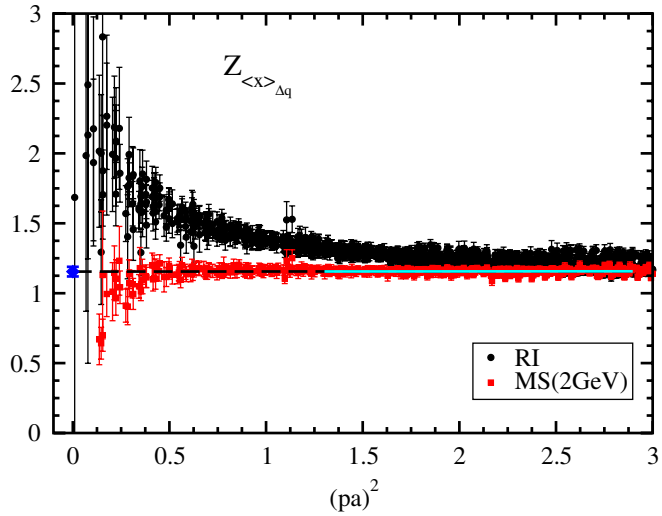

FIG. 8 (color online). Nonperturbative renormalization for the quark helicity fraction, $\langle x \rangle_{\Delta u - \Delta d}$. Circles denote the RI-MOM values, and squares denote the $\overline{\mathrm{MS}}$ ones. The line denotes a linear fit used to remove the leading $O((ap)^2)$ lattice artifacts.

With this renormalization, $\langle x \rangle_{\Delta u - \Delta d}$ can be compared with the experiment (see Fig. 9 and Table V). No finite-volume effect is apparent in the data, similar to the quark momentum fraction. The three heavier-mass results from the smaller volume again agree with the respective larger-mass results, suggesting the huge finite-size effect, seen in the elastic form factors, that appears to scale with $m_\pi L$, is not present in this moment of this deep-inelastic structure function, at least at the quark masses considered here.

Moreover, the observable exhibits very similar quark-mass dependence to the momentum fraction, as can be expected from the near constant behavior of their ratio: the three heavier points stay roughly the constant and about 70% higher than the experimental value, and the lightest point shows a sign of deviation away from this constant behavior. This trend toward the experimental value may be a real physical effect.

Here, we note that while our results of $\langle x \rangle_{u-d}$ are in agreement with $n_f = 2$ Wilson results [49], they differ significantly from the LHP mixed-action calculations [50]. Their values are significantly lower, by about 20%. The main source of this discrepancy is likely due to the use of perturbative renormalization by the LHP Collaboration. In the LHP mixed-action calculations [50], the renormalization constant is evaluated by $Z_{\mathcal{O}} = (Z_{\mathcal{O}}/Z_A)^{\mathrm{pert}} \times Z_A^{\mathrm{nonpert}}$ for the operator $\mathcal{O}$. In the same manner, we use the value of $(Z_{\mathcal{O}}/Z_A)^{\mathrm{pert}}$ for the operator $\mathcal{O}^{5q}_{\{34\}}$ from Ref. [51] and $Z_A^{\text{non-pert}} = 0.7161(1)$ from Ref. [1], and

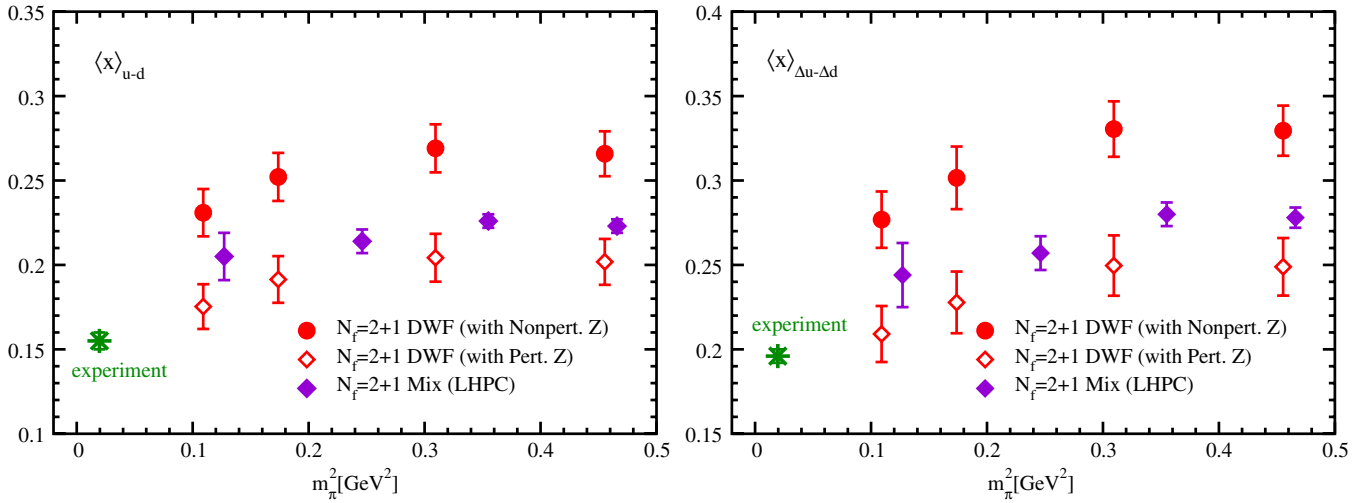

FIG. 10 (color online). Comparison with results obtained from the mixed-action calculation [50] of the LHP Collaboration (filled diamonds). The left (right) panel is for the renormalized value of quark momentum (helicity) fraction. Our fully nonperturbatively renormalized results are represented by filled circles, while open diamonds denote our estimates of the same quantity with the renormalization constant determined perturbatively.

evolve it to a renormalization scale of 2 GeV using the two-loop anomalous dimension [26,31], obtaining the renormalization factor $Z_{\langle x\rangle_{\Delta q}}(2\ \mathrm{GeV}) = 0.873(34)$ in the $\overline{\mathrm{MS}}$ scheme.

If we use this renormalization factor instead of the nonperturbative one described earlier, as shown in Fig. 10, our results will be consistent with the LHPC results. The difference between the nonperturbative and perturbative renormalization factors suggests a systematic error of about 25% should be assigned to the latter. Furthermore, those lightest points in both quark momentum and helicity fractions are quite close to the experiments, while the nonperturbatively renormalized ones are significantly away from the experiments. This indicates that the perturbative calculation of the renormalization constants significantly underestimates the renormalized value of these particular quantities, and then exhibits an accidental consistency with the experiments.

As mentioned before, it is observed that there is a noticeable nonlinearity in the data of both $\langle x\rangle_{u-d}$ and $\langle x\rangle_{\Delta u-\Delta d}$. These trends toward the experimental values are easily seen in Fig. 11, where the (2 + 1)-flavor and previous RBC quenched [25] and 2-flavor [26] results are plotted together with the leading nonlinear behavior predicted in heavy baryon chiral perturbation theory (HBChPT) [52–54]:

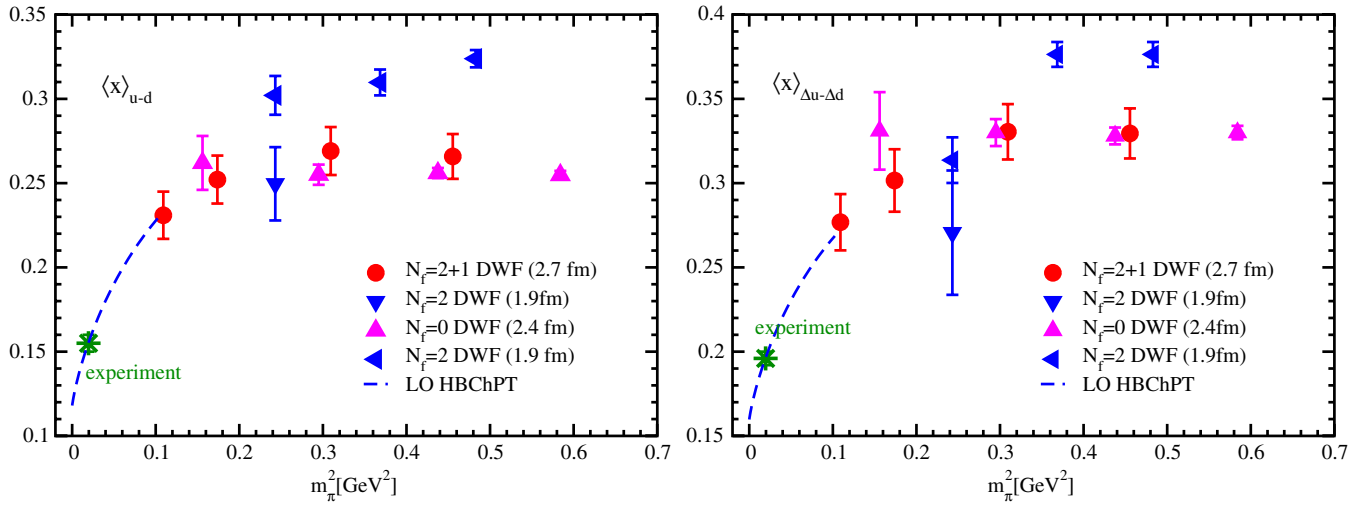

FIG. 11 (color online). Comparison with previous RBC quenched [25] and 2-flavor [26] results. The left triangles denote 2-flavor points with a time separation between source and sink of 12 sites instead of 10 (down triangles). Dashed curves show the leading order behavior in HBChPT in the vicinity of the physical pion mass point.

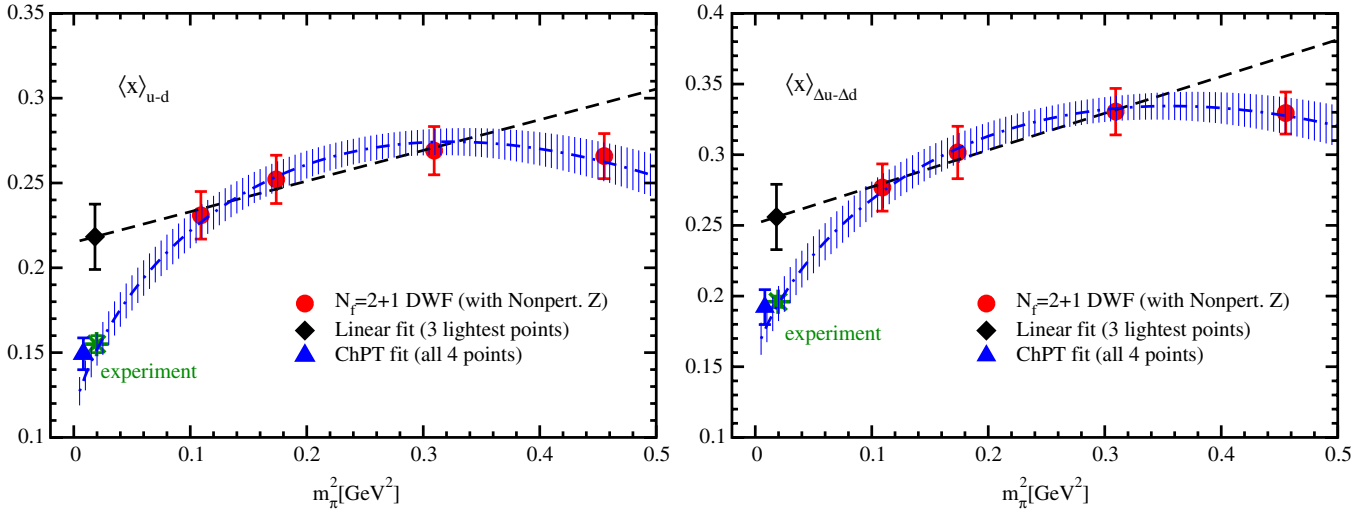

FIG. 12 (color online). Linear and leading HBChPT fits to the nonperturbatively renormalized quark momentum fraction, $\langle x\rangle_{u-d}$, and helicity fraction, $\langle x\rangle_{\Delta u-\Delta d}$. The three lightest data points are used in the former, and all four in the latter. The diamond and triangle denote extrapolated values at the physical point. The triangles have been shifted slightly to the left for clarity.

$$\langle x\rangle_{u-d} = C\left[1 - \frac{3g_A^2+1}{(4\pi F_\pi)^2} m_\pi^2 \ln\left(\frac{m_\pi^2}{\Lambda^2}\right)\right] + e(\Lambda^2)\frac{m_\pi^2}{(4\pi F_\pi)^2}, \tag{18}$$

$$\langle x\rangle_{\Delta u-\Delta d} = \tilde{C}\left[1 - \frac{2g_A^2+1}{(4\pi F_\pi)^2} m_\pi^2 \ln\left(\frac{m_\pi^2}{\Lambda^2}\right)\right] + \tilde{e}(\Lambda^2)\frac{m_\pi^2}{(4\pi F_\pi)^2}. \tag{19}$$

Although our lightest point may be beyond the applicability of HBChPT,[1] the downward trends are expected to develop at least in the vicinity of the physical pion mass point. As a simple prediction, the curve is shown using experimental values for the nucleon axial charge and pion decay constant, $g_A = 1.269$ and $F_\pi = 92.8$ MeV, a chiral scale $\Lambda = m_N = 940$ MeV, and by setting the unknown low energy constants to zero, $e(\Lambda) = \tilde{e}(\Lambda) = 0$. The values in the chiral limit are obtained by requiring the curves to agree with experiment at the physical point. It is interesting to note that the quenched results show no hint of this behavior, while the 2-flavor ones are inconclusive. We remind the reader that for the 2-flavor data, a smaller time separation between sources, $t_{\rm sep} \approx 1.16$ fm, was used. When the separation was increased for the lightest mass, the momentum and helicity fractions drop, but with a significant increase in the statistical error.

Physical point values $\langle x\rangle_{u-d} = 0.218(19)$ and $\langle x\rangle_{\Delta u-\Delta d} = 0.256(23)$, determined by simple linear chiral extrapolation of the three lightest points, overshoot the experimental ones by more than 2–3 standard deviations, as shown in Fig. 12. On the other hand, the HBChPT fit forms in Eqs. (18) and (19) with the experimental values of g_A and F_π accommodate all four data points and produce extrapolations in good agreement with the respective experimental values[2] (see Fig. 12). Fits to only the lightest three points, or with $g_A = 1.0$, do not significantly alter the results. We caution that at this stage these fits, and associated values of the low energy constants, represent little more than "phenomenological" fits to our data as the pion masses used are relatively heavy and most, if not all, are likely beyond the applicable range of HBChPT. Although these extrapolations indicate a favorable trend, definitive results require simulations with several lighter quark masses than our lightest one. All fits are summarized in Table VI.

B. Transversity (Tensor charge)

Results for the bare isovector tensor charge, $\langle 1\rangle_{\delta u-\delta d}$, are presented in Fig. 13, and in Fig. 14 we present its nonperturbative renormalization constant. We obtain a renormalization factor of $Z^{\overline{\rm MS}}(2\ {\rm GeV}) = 0.783(6)$. The error is statistical and systematic from rotational symmetry breaking, and each contributes equally. However, note that the total error is still less than 1%.

Combining them, we obtain the renormalized tensor charge as presented in Fig. 15 and summarized in Table V. These provide a rough physical prediction which is still worthwhile since the experiments are yet to report a value. If we fit the heavy three points with a constant, we obtain a value of about 1.10(7). Alternatively, if we linearly

[1]It can be observed in some particular cases like the nucleon axial charge g_A and the nucleon root-mean-squared charge radius [26,27].

[2]The experimental values were determined using a tool from CTEQ [55] and data from [14,17,19].

TABLE V. Isovector combination $(u-d)$ of the quark momentum fraction $\langle x\rangle_q$, helicity fraction $\langle x\rangle_{\Delta q}$, and transversity $\langle 1\rangle_{\delta q}$, nonperturbatively renormalized in the $\overline{\text{MS}}$ scheme at 2 GeV.

m_f	$\langle x\rangle^{\overline{\text{MS}}}_{u-d}$ (2 GeV)	$\langle x\rangle^{\overline{\text{MS}}}_{\Delta u-\Delta d}$ (2 GeV)	$\langle 1\rangle^{\overline{\text{MS}}}_{\delta u-\delta d}$ (2 GeV)
0.005	0.231(14)	0.277(17)	0.990(35)
0.01	0.252(14)	0.302(19)	1.126(32)
0.02	0.269(14)	0.330(16)	1.084(30)
0.03	0.266(13)	0.329(15)	1.132(25)

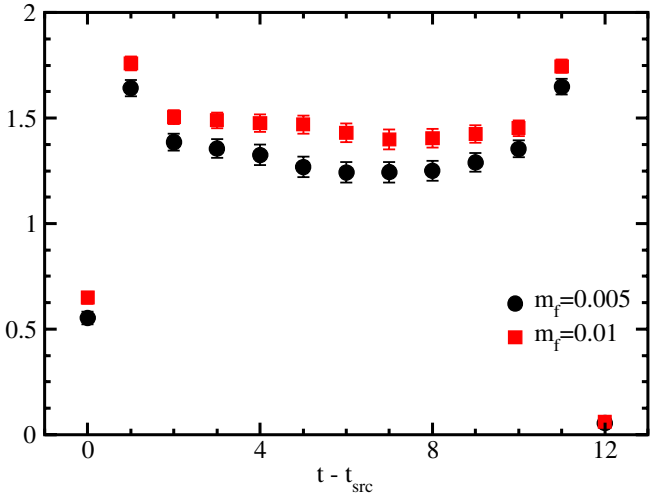

FIG. 13 (color online). Signals for the ratio of three- and two-point functions for the bare quark transversity, $\langle 1\rangle_{\delta u-\delta d}$. Quark mass 0.005 (circles) and 0.01 (squares).

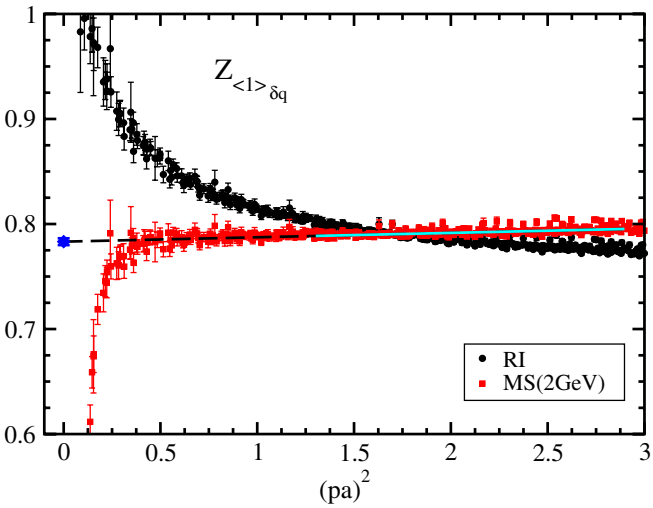

FIG. 14 (color online). Nonperturbative renormalization for the quark transversity, $\langle 1\rangle_{\delta u-\delta d}$. Circles denote the RI-MOM values, squares the $\overline{\text{MS}}$ ones. The line denotes a linear fit used to remove the leading $O((ap)^2)$ lattice artifacts.

TABLE VI. Summary of extrapolations to the physical point of the renormalized first moment of the quark momentum and helicity fractions. Physical values are given at a scale of $\mu = 2$ GeV. The chiral scale in the HBChPT fits is $\Lambda = 0.94$ GeV. The slope in the linear fit is in units of $1/(4\pi F_\pi)^2$. "LEC" stands for low energy constant; i.e., C in Eq. (18) is LEC 1, and $e(\Lambda)$ is LEC 2.

Moment			χ^2/dof	Phys. val.	Exp. val.
	HBChPT fit				
	LEC 1	LEC 2			
$\langle x\rangle^{\overline{\text{MS}}}_{u-d}$	0.1145(77)	0.001(77)	0.14	0.1493(94)	0.154(3)
$\langle x\rangle^{\overline{\text{MS}}}_{\Delta u-\Delta d}$	0.157(11)	0.073(89)	0.03	0.192(12)	0.196(4)
	Linear fit				
	Intercept	Slope			
$\langle x\rangle^{\overline{\text{MS}}}_{u-d}$	0.215(21)	0.25(13)	0.25	0.218(19)	
$\langle x\rangle^{\overline{\text{MS}}}_{\Delta u-\Delta d}$	0.251(25)	0.34(16)	0.11	0.256(23)	

extrapolate the two lightest points we would obtain about 0.7.

C. Twist-3 moment

Figure 16 presents the bare lattice signals for the twist-3 moment, d_1, of the polarized structure function g_2. They are summarized in Table VII.

We have not yet computed the renormalization constant for this quantity. The quark-mass dependence of the bare values are presented in Fig. 17. Our interest here is in whether the perturbatively obtained Wandzura-Wilczek relation [56] holds. From the smallness of the values obtained, we conclude that it does. We note that our results indicate that the lightest mass points deviate slightly from the linear trends set by the heavier points.

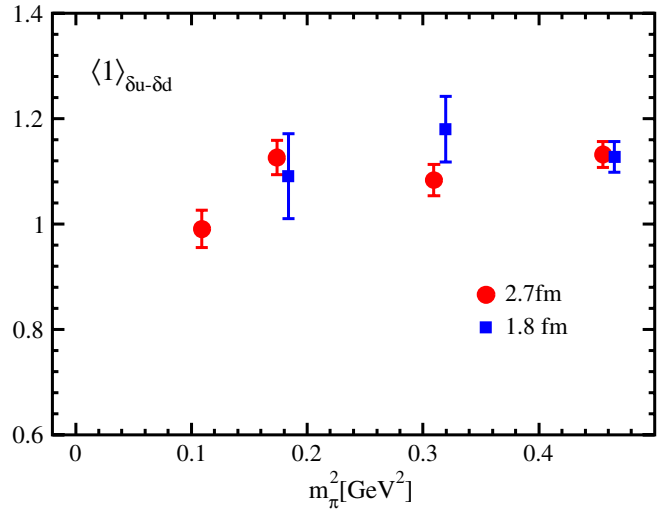

FIG. 15 (color online). Renormalizaed tensor charge, $\langle 1\rangle_{\delta u-\delta d}$. Both volumes are shown, $(2.7\text{ fm})^3$ (circles) and $(1.8\text{ fm})^3$ (squares). The square symbols have been moved slightly in the plus x direction for clarity.

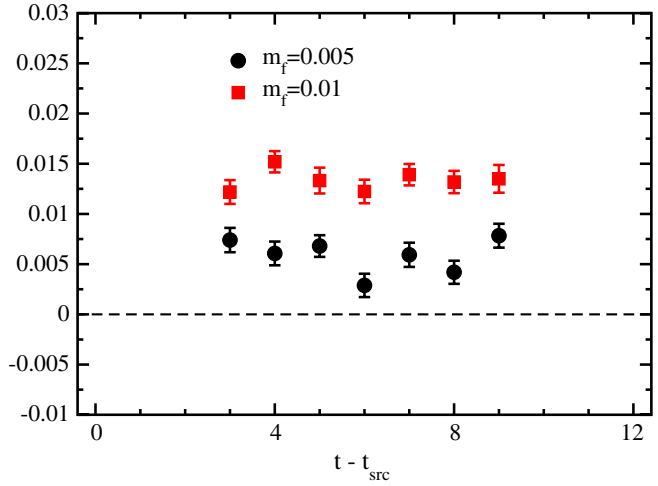

FIG. 16 (color online). Bare signals from the ratio of three- and two-point function for twist-3 moment, d_1, for $m_f = 0.005$ and 0.01.

TABLE VII. Bare twist-3 first moment of the polarized structure function, d_1, on the $(2.7\ \mathrm{fm})^3$ ensemble.

m_f	d_1^{u-d}	d_1^u	d_1^d
0.005	0.0052(3)	0.0038(3)	−0.0013(2)
0.01	0.0137(4)	0.0108(4)	−0.0029(3)
0.02	0.0273(8)	0.0219(8)	−0.0055(4)
0.03	0.0422(9)	0.0338(9)	−0.0085(5)

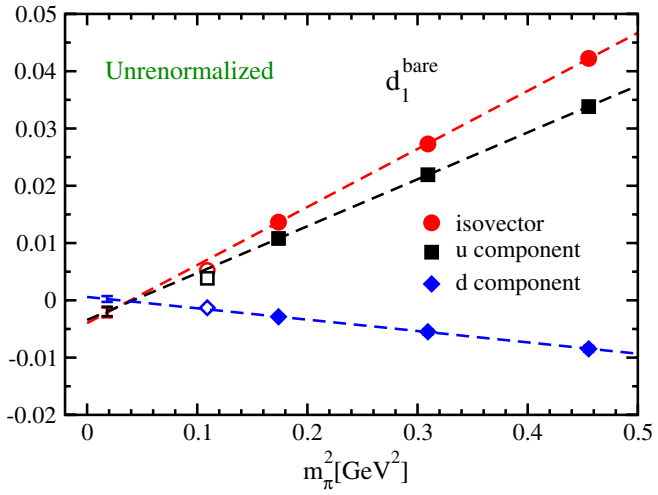

FIG. 17 (color online). Bare values of the twist-3 moment d_1, with linear extrapolation to the physical point, excluding the lightest point (open symbols). Up quark contribution (squares), down quark contribution (diamonds), and the isovector combination (circles) are shown. 24^3 ensemble.

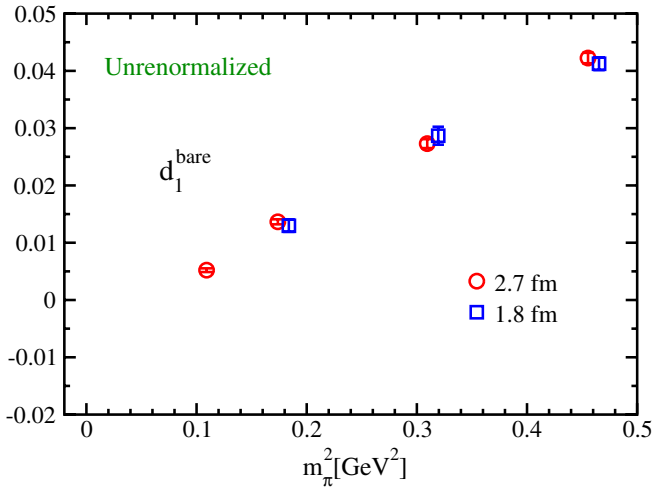

FIG. 18 (color online). The twist-3 lowest moment of the polarized structure function d_1 (not renormalized). Both volumes are shown, $(2.7\ \mathrm{fm})^3$ (circles) and $(1.8\ \mathrm{fm})^3$ (squares). The square symbols have been moved slightly in the plus x direction for clarity.

In Fig. 18 values on different volumes are compared. d_1 appears to be insensitive to finite-volume effects, at least in this range of light quark masses.

V. CONCLUSIONS

We have presented calculations of some of the lowest moments of nucleon structure functions in (2 + 1)-flavor QCD, using domain-wall fermions and the Iwasaki gauge action. The calculations were carried out on two volumes at a single lattice spacing ($a^{-1} = 1.73$ GeV) with quark masses that yield pion masses in the range 0.33 to 0.67 GeV. The results are encouraging.

The ratio of the bare quark momentum and helicity fractions, which is automatically renormalized, is found to be independent of the light quark mass through the range of our calculations, $\frac{1}{5} m_{\mathrm{strange}} \leq m_{\mathrm{ud}} \leq \frac{3}{4} m_{\mathrm{strange}}$, and agrees with the value obtained from experiment within statistical error. This is in contrast to a similarly automatically renormalized ratio—g_A/g_V, of the isovector, axial-vector, and vector charges—that is severely distorted by the finite size of the lattice [27,39] at the lightest quark mass.

This suggests the corresponding downward trend toward the experimental values, as the quark mass decreases, of both the momentum, $\langle x \rangle_{u-d}$, and helicity, $\langle x \rangle_{\Delta u - \Delta d}$, fractions is a real physical effect. Comparison of these results on two different volumes supports this observation. In fact, all of the moments studied here agree well, within statistical errors, on two different volumes, $(2.7\ \mathrm{fm})^3$ and $(1.8\ \mathrm{fm})^3$.

In addition to the momentum and helicity fractions, the nonperturbatively renormalized tensor charge, $\langle 1 \rangle_{\delta u - \delta d}$, has been computed. The chiral extrapolation, in particular,

needs to be understood before an accurate prediction can be made. Since upcoming experiments have yet to report a value, we give a rough estimate, from two different chiral extrapolations, that its value lies in the range 0.7–1.1.

The twist-3 moment of the g_2 structure function, d_1, is also obtained. Though yet to be renormalized, its smallness suggests the Wandzura-Wilczek relation holds.

The possibility that the long sought curvature of the moments in the chiral regime is becoming visible in our results has encouraged us to start calculations at even smaller quark masses ($m_\pi \approx 250$ and 180 MeV), on an even larger lattice ($L \approx 4.5$ fm). This ensemble, which is being generated by the RBC and UKQCD Collaborations [57], was conceived, in part, to attain these goals for nucleon matrix elements.

ACKNOWLEDGMENTS

We thank the members of the RBC and UKQCD Collaborations. H. L. is supported by the U.S. D.O.E. under Grant No. DE-FG03-97ER4014 and J. Z. by STFC Grant No. ST/F009658/1. S. O. thanks the RIKEN-BNL Research Center for partial support. S. S. is supported by the JSPS for a Grant-in-Aid for Scientific Research (C), Grant No. 19540265, T. B. by the U.S. D.O.E. under Contract No. DE-FG02-92ER40716, and Y. A. by the JSPS for a Grant-in-Aid for Scientific Research (C), Grant No. 21540289. RIKEN, BNL, the U.S. D.O.E., Edinburgh University, and the UK PPARC provided facilities essential for this work. The computations reported here were carried out on the QCDOC supercomputers at the RBRC and the University of Edinburgh.

[1] C. Allton *et al.* (RBC-UKQCD Collaboration), Phys. Rev. D **78**, 114509 (2008).
[2] D. B. Kaplan, Phys. Lett. B **288**, 342 (1992).
[3] Y. Shamir, Nucl. Phys. **B406**, 90 (1993).
[4] V. Furman and Y. Shamir, Nucl. Phys. **B439**, 54 (1995).
[5] J. M. Zanotti, Proc. Sci., LAT2008 (2008) 007.
[6] P. Hagler, Phys. Rep. **490**, 49 (2010).
[7] D. B. Renner, arXiv:1002.0925.
[8] M. Breidenbach *et al.*, Phys. Rev. Lett. **23**, 935 (1969).
[9] J. I. Friedman, Rev. Mod. Phys. **63**, 615 (1991).
[10] H. W. Kendall, Rev. Mod. Phys. **63**, 597 (1991).
[11] R. E. Taylor, Rev. Mod. Phys. **63**, 573 (1991).
[12] M. Gluck, E. Reya, M. Stratmann, and W. Vogelsang, Phys. Rev. D **53**, 4775 (1996).
[13] T. Gehrmann and W. J. Stirling, Phys. Rev. D **53**, 6100 (1996).
[14] H. L. Lai *et al.*, Phys. Rev. D **55**, 1280 (1997).
[15] D. Adams *et al.* [Spin Muon (SMC)], Phys. Rev. D **56**, 5330 (1997).
[16] B. Adeva *et al.* (Spin Muon), Phys. Lett. B **420**, 180 (1998).
[17] M. Gluck, E. Reya, and A. Vogt, Eur. Phys. J. C **5**, 461 (1998).
[18] K. Ackersta *et al.* (HERMES), Phys. Lett. B **464**, 123 (1999).
[19] A. D. Martin, R. G. Roberts, W. J. Stirling, and R. S. Thorne, Eur. Phys. J. C **23**, 73 (2002).
[20] M. Anselmino *et al.*, Phys. Rev. D **75**, 054032 (2007).
[21] RHIC Collaboration (2008), http://spin.riken.bnl.gov/rsc/report/spinplan_2008/spinplan08.pdf.
[22] T. Yamazaki and S. Ohta (RBC and UKQCD Collaborations), Proc. Sci., LAT2007 (2007) 165.
[23] S. Ohta and T. Yamazaki (RBC and UKQCD Collaborations), Proc. Sci., LATTICE2008 (2008) 168.
[24] S. Ohta (RBC and UKQCD Collaborations), arXiv:0910.5686.
[25] K. Orginos, T. Blum, and S. Ohta (RBC Collaboration), Phys. Rev. D **73**, 094503 (2006).
[26] H.-W. Lin, T. Blum, S. Ohta, S. Sasaki, and T. Yamazaki (RBC Collaboration), Phys. Rev. D **78**, 014505 (2008).
[27] T. Yamazaki *et al.*, Phys. Rev. D **79**, 114505 (2009).
[28] G. Martinelli, C. Pittori, C. T. Sachrajda, M. Testa, and A. Vladikas, Nucl. Phys. **B445**, 81 (1995).
[29] C. Dawson *et al.*, Nucl. Phys. **B514**, 313 (1998).
[30] M. Gockeler *et al.*, Nucl. Phys. **B544**, 699 (1999).
[31] E. G. Floratos, D. A. Ross, and C. T. Sachrajda, Nucl. Phys. **B129**, 66 (1977); **B139**, 545(E) (1978).
[32] T. van Ritbergen, J. A. M. Vermaseren, and S. A. Larin, Phys. Lett. B **400**, 379 (1997).
[33] W. M. Yao *et al.* (Particle Data Group), J. Phys. G **33**, 1 (2006).
[34] Y. Aoki *et al.*, Phys. Rev. D **78**, 054510 (2008).
[35] D. J. Broadhurst and A. G. Grozin, Phys. Rev. D **52**, 4082 (1995).
[36] Y. Iwasaki, Report No. UTHEP-118, 1983 (unpublished).
[37] C. Alexandrou, S. Gusken, F. Jegerlehner, K. Schilling, and R. Sommer, Nucl. Phys. **B414**, 815 (1994).
[38] F. Berruto, T. Blum, K. Orginos, and A. Soni, Phys. Rev. D **73**, 054509 (2006).
[39] T. Yamazaki *et al.* (RBC and UKQCD Collaborations), Phys. Rev. Lett. **100**, 171602 (2008).
[40] W. Detmold, W. Melnitchouk, and A. W. Thomas, Mod. Phys. Lett. A **18**, 2681 (2003).
[41] W. Detmold and C. J. D. Lin, Proc. Sci., LAT2005 (2006) 361.
[42] J. D. Bratt *et al.* (LHPC Collaboration), arXiv:1001.3620.
[43] C. Kelly, P. A. Boyle, and C. T. Sachrajda (RBC Collaboration), Proc. Sci., LAT2009 (2009) 087.
[44] R. Mawhinney (RBC Collaboration), Proc. Sci., LAT2009 (2009) 081.
[45] Y. Aoki, Proc. Sci., LAT2009 (2009) 012.
[46] M. Constantinou, V. Lubicz, H. Panagopoulos, and F. Stylianou, J. High Energy Phys. 10 (2009) 064.
[47] M. Constantinou *et al.*, arXiv:1004.1115.
[48] M. Gockeler *et al.*, arXiv:1003.5756.
[49] M. Gockeler *et al.*, arXiv:0912.0167.

[50] P. Hagler *et al.* (LHPC Collaboration), Phys. Rev. D **77**, 094502 (2008).
[51] P. A. Boyle *et al.* (UKQCD Collaboration), Phys. Lett. B **641**, 67 (2006).
[52] J.-W. Chen and X.-d. Ji,Phys. Lett. B **523**, 73 (2001).
[53] D. Arndt andM. J. Savage, Nucl. Phys. **A697**, 429 (2002).
[54] W. Detmold, W. Melnitchouk, and A. W. Thomas, Phys. Rev. D **66**, 054501 (2002).
[55] J. Pumplin *et al.*, J. High Energy Phys. 07 (2002) 012.
[56] S. Wandzura and F. Wilczek, Phys. Lett. **72B**, 195 (1977).
[57] C. Jung, arXiv:1001.0941.